ELSEVIER

Polymer 42 (2001) 5749–5754

polymer

www.elsevier.nl/locate/polymer

Crystallization induced microstructure of crystalline/crystalline poly(vinylidenefluoride)/poly(3-hydroxybutyrate) blends probed by small angle X-ray scattering

H.-J. Chiu[a], H.-L. Chen[a,*], J.S. Lin[b]

[a]*Department of Chemical Engineering, National Tsing Hua University, Hsin-Chu, 30013 Taiwan, ROC*
[b]*Solid State Division, Oak Ridge National Laboratory, Oak Ridge, Tennessee 37831, USA*

Received 23 October 2000; received in revised form 11 December 2000; accepted 22 December 2000

Abstract

The lamellar morphology of a melt-miscible blend consisting of two crystalline constituents, poly(vinylidene fluoride) (PVDF) and poly(3-hydroxybutyrate) (PHB), has been investigated by small angle X-ray scattering (SAXS). Owing to the proximity of melting points, PVDF and PHB crystallized over essentially the same temperature range, and consequently created a crystalline/crystalline state with the morphology characterized by the spatial arrangement of PVDF and PHB lamellae. Irrespective of the crystallization temperatures (T_c), the SAXS patterns revealed the presences of two lamellar stack (LS) domains, where one contained mainly PVDF lamellae (PVDF LS domain) and the other primarily consisted of PHB lamellae (PHB LS domain). The interlamellar (IL) regions of both LS domains were found to contain mixed amorphous PVDF and PHB. The blends crystallized at higher T_c exhibited smaller SAXS invariants. This observed T_c dependence was connected with the disparity in crystallization kinetics that gave rise to different LS domain sizes at different T_cs.

Keywords: Blends; Morphology; Crystallization

1. Introduction

Binary polymer blends can be classified into amorphous/amorphous, crystalline/amorphous, and crystalline/crystalline systems based on the crystallizability of the constituents. For the later two systems, where at least one component is crystallizable, the occurrence of liquid–solid phase separation can generate a wide variety of morphological patterns [1]. In a melt-miscible crystalline/amorphous blend, for example, crystallization is accompanied with the segregation of the amorphous diluent. The morphological structure is characterized by the distance over which the diluent is segregated, where the diluent may be expelled into the interlamellar (IL segregation), interfibrillar (IF segregation), or interspherulitic (IS segregation) regions. These morphological patterns represent the diluent dispersion from nanoscopic scale for IL segregation to micrometer scale for IS segregation. Different scales of dispersion may lead to different properties.

For crystalline/crystalline systems where cocrystallization is absent, crystallization of the two components creates two crystal species (A and B). The morphology is characterized by the spatial arrangement of the two crystal species, where the pattern can be divided into the 'insertion mode' where A and B crystals mix in the lamellar stack (LS) and the 'block mode' where A and B crystals form respective LS domains [2–3]. These morphological patterns are governed by the mutual exclusion distance of the two components during crystallization [2–5]. Insertion mode is induced by the mutual segregation distance comparable to the lamellar thickness, which is in the order of several nm. Block mode is characterized by the longer segregation distance, in the order of tens of nm to μm.

The microstructure of crystalline/amorphous blends has been well studied over the past few decades. On the other hand, because only a limited number of systems have been disclosed so far, the mechanism associated with the microstructure formation in crystalline/crystalline systems is still far from well understood. The most widely studied crystalline/crystalline system is perhaps the blends of high-density polyethylene (HDPE) and low-density polyethylene (LDPE) (e.g. Refs. [6–13]). This binary pair represents an 'ideal' (yet complex) system in the sense that the effect of

* Corresponding author. Tel.: +886-3-5721714; fax: +886-3-5715408.
E-mail address: hlchen@che.nthu.edu.tw (H.-L. Chen).

0032-3861/01/$ - see front matter
PII: S0032-3861(01)00072-6

unlike intermolecular interaction is nil. Other crystalline/crystalline blends such as polycarbonate (PC)/polycaprolactone (PCL) [4,5,14,15]], poly(ethylene terephthalate) (PET)/poly(butylene terephthalate) (PBT) [16], poly(vinylidene fluoride) (PVDF)/poly(butylene adipate) (PBA) [17–20], poly(3-hydroxybutyrate) (PHB)/poly(ethylene oxide) (PEO) [21–23], and PBT/polyarylates (PAr) [24], and PEO/poly(ethylene succinate) (PES) have been reported. PC/PCL, PVDF/PBA, and PEO/PES are the systems whose morphological structures have been characterized in the lamellar level.

In this paper, the morphological pattern of a crystalline/crystalline system consisting of PVDF and PHB is reported. PVDF and PHB are both crystalline polymers having the observed melting points (T_m) of ca. 170°C. PVDF and PHB had been found to form a miscible blend above T_m [25,26]. At $T < T_m$, both PVDF and PHB may undergo crystallization but they do not cocrystallize into the same crystal lattice owing to the large differences in crystalline chain conformation and crystallization kinetics. In the present study, the morphological structures of PVDF/PHB generated at three crystallization temperatures ($T_c = 70$, 125, and 146°C) are probed by small angle X-ray scattering (SAXS). The morphological patterns in the lamellar level are deduced from the SAXS profiles, invariant, and the one-dimensional correlation function analysis. It will be shown that the disparity in crystallization kinetics plays an important role in the microstructure formation of crystalline/crystalline polymer blends.

2. Experimental

2.1. Materials and sample preparation

PVDF with molecular weight of 60,000 was purchased from Polysciences and PHB with $M_n = 2.93 \times 10^5$ and $M_w = 6.5 \times 10^5$ was acquired from Aldrich. Blendings of PVDF and PHB were carried out by solution casting. The blending components were dissolved in DMF at room temperature yielding a 1 wt% solution. The solution was subsequently poured onto a petri dish and the blend film was obtained after evaporating most solvent on a hot plate at ca. 90°C. The blend film was further dried in vacuo at 90°C for 24 h.

Specimens for SAXS study were prepared by pressing the blends between two pieces of Teflon films on a Linkam HFS91 hot stage at 190 ± 0.2°C for 1 min, followed by quickly transferring the samples into an oven equilibrated at the desired crystallization temperatures ($T_c = 70$, 125 and 146°C). The crystallizations were allowed to proceed for 72 h.

2.2. SAXS measurement

SAXS experiments were performed at room temperature on the Oak Ridge National Laboratory (ORNL) 10-m SAXS instrument, with a sample-to-detector distance of 5 and 2 m using CuK_α radiation ($\lambda = 1.54$ Å) and a 20×20 cm^2 two-dimensional position-sensitive detector with each virtual cell element of about 3 mm apart. The scattering intensity was stored in a 64×64 data array. Corrections were made for instrumental backgrounds, dark current due to cosmic radiation and electronic noises, and detector non-uniformity and efficiency (via an Fe^{55} radioactive standard which emits γ-rays isotropically) on a cell-by-cell basis. The data were radially (azimuthually) averaged in the q range: $0.1\ \text{nm}^{-1} < q < 2.5\ \text{nm}^{-1}$, ($q = 4\pi/\lambda\ \sin(\theta/2)$, where λ is the X-ray wavelength and θ is the scattering angle), and converted to an absolute differential scattering cross section by means of pre-calibrated secondary standard [27].

3. Results and discussion

Isothermal crystallizations at three temperatures, $T_c = 70$, 125, and 146°C, were conducted to generate the crystalline/crystalline states of PVDF/PHB blends. Although both PVDF and PHB were able to crystallize in the T_c range investigated, their crystallization rates were very different in that the crystallization of PVDF always occurred prior to that of PHB [25–26]. The disparity in crystallization kinetics became increasingly evident at higher T_c.

Fig. 1 displays the Lorentz-corrected SAXS profiles in absolute intensity unit of PVDF/PHB crystallized at three T_cs. Neat PVDF shows a stronger scattering peak than neat PHB because of higher electron density contrast between the alternating crystalline and amorphous layers ($\Delta\eta(\text{PVDF}) = 0.103$ mol cm^{-3}; $\Delta\eta(\text{PHB}) = 0.050$ mol cm^{-3}) [28–31]. Irrespective of the T_cs, a shoulder (marked by the arrows) beside the main peak is identified for the blends with its intensity growing with increasing PHB composition. For these compositions, the overall scattering profiles can be represented by the superposition of a main peak located at 0.2–0.35 nm^{-1} and a minor peak at 0.6–0.8 nm^{-1}. These two scattering peaks imply the existence of two LS domains in the crystalline/crystalline blends. The low-q peak is associated with the LS domains primarily consisting of PVDF lamellae (PVDF LS domain) and the high-q peak is attributed to the LS domains containing mainly PHB lamellae (PHB LS domain). Therefore, the morphological pattern of crystalline/crystalline PVDF/PHB is represented by the block mode of lamellar arrangement.

The low-q peak associated with the PVDF LS domains shifts toward lower q and its intensity grows upon blending with PHB. The intensity enhancement is particularly evident for the PVDF-rich compositions ($w_{PHB} < 0.5$), while the intensity diminishes for the PHB-rich blends because of the lower volume fraction of the PVDF LS domains. Enhancement of scattering intensity is ascribed to the incorporation of uncrystalline PHB in the regions between the individual PVDF lamellae (i.e. the IL regions) in the PVDF

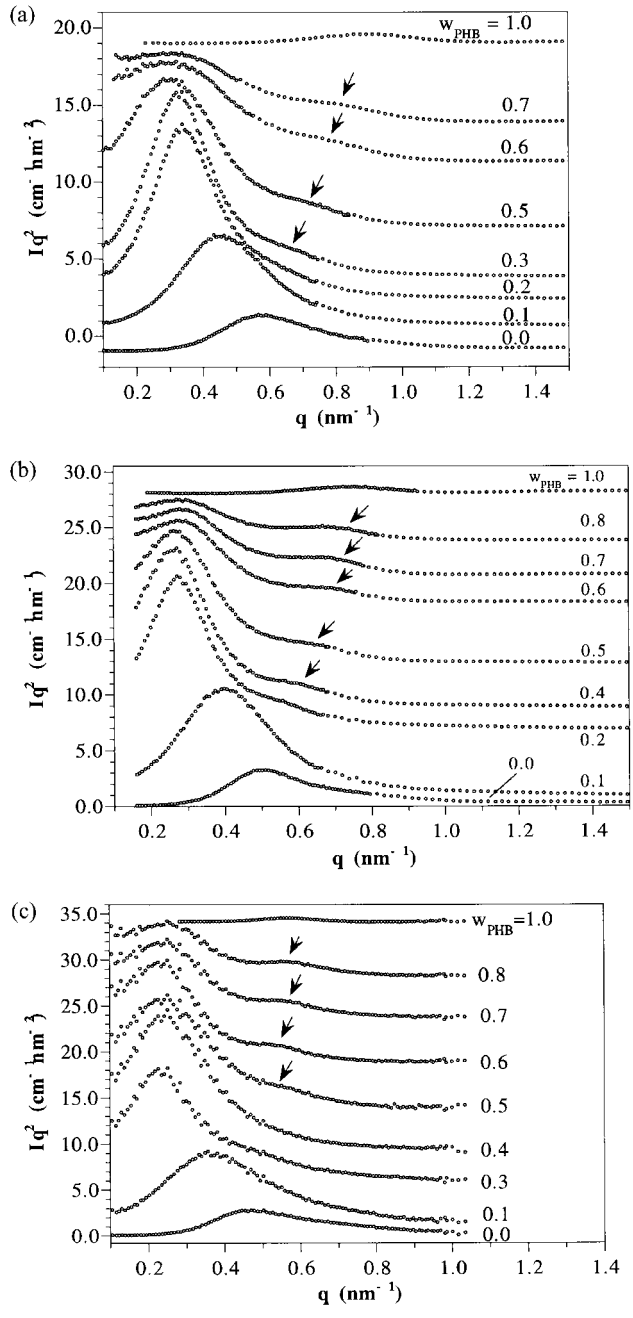

Fig. 1. Lorentz-corrected SAXS profiles of PVDF/PHB after crystallized at T_c = (a) 70, (b) 125, and (c) 146°C for 72 h. The arrows indicate the scattering contribution from the PHB LS domains. The scattering curves of the blends are displaced vertically for clear comparison.

LS domains. Since the electron density of amorphous PHB (0.630 mol cm^{-3}) is much lower than that of amorphous PVDF (0.833 mol cm^{-3}), the mixing of amorphous PHB with uncrystalline PVDF in the IL regions would inevitably enhance the electron density contrast between the crystalline and amorphous layers and consequently gives rise to stronger scattering intensity.

Fig. 2 presents the composition variation of the weight-average long period (L_B) of the PVDF LS domains calculated from the peak position (q_{max}) using Bragg's equation ($L_B = 2\pi/q_{max}$). The composition dependence of L_B appears the same for all T_cs investigated, where the long period increases upon blending with PHB but the swelling reaches a 'saturation' when the overall PHB composition exceeds 30 wt%. Swelling of long period may further support the incorporation of PHB in the IL regions of the PVDF LS domains. Fig. 3 plots the composition variation of the L_B of PHB LS domains estimated from the positions of the shoulders in Fig. 1. The long period also swells upon blending with PVDF, which may imply the incorporation of uncrystalline PVDF in the IL regions of the PHB LS domains.

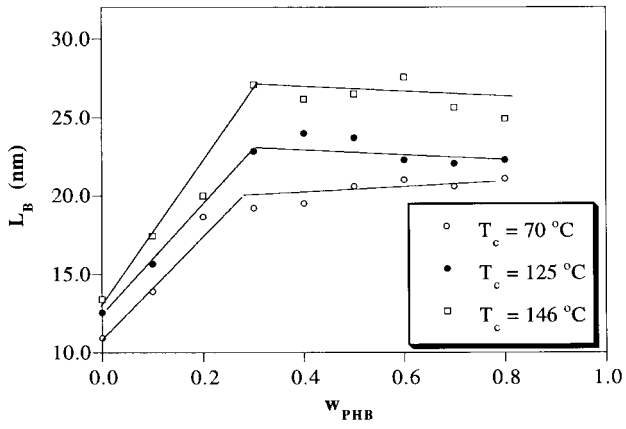

Fig. 2. Composition variation of the weight-average long period (L_B) of the PVDF LS domains calculated by the Bragg's equation ($L_B = 2\pi/q_{max}$).

The long period represents the sum of the crystalline and amorphous layer thickness. Deconvolution into the thickness of these two types of layers can be accomplished using the one-dimensional correlation function. The correlation function, $K(z)$, defined by Strobl and Schneider, adopts the following form [32]:

$$K(z) = \frac{1}{2\pi^2}\int_0^\infty Iq^2 \cos qz \, dq, \quad (1)$$

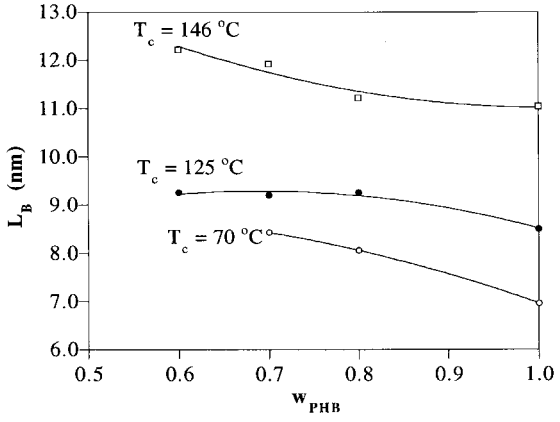

Fig. 3. The weight-average long period of the PHB LS domains estimated from the positions of the shoulders in Fig. 1.

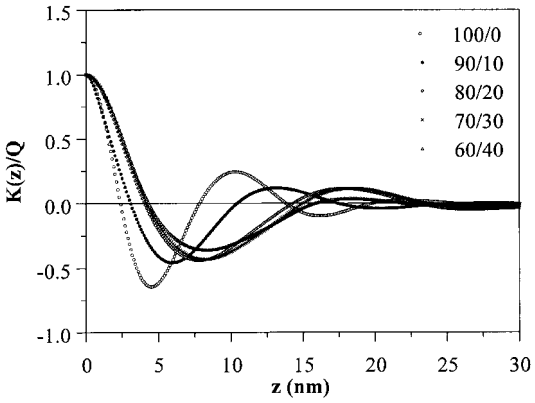

Fig. 4. One-dimensional correlation functions of PVDF/PHB blends crystallized at 70°C. The correlation functions have been normalized by the invariant (Q) for better comparison.

where I is the absolute intensity. Since the shoulder scattering associated with the PHB LS domain was hardly identified for PVDF-rich compositions ($w_{PHB} \leq 0.4$), it is reasonable to assume that the shape of $K(z)$ associated with the PVDF LS domains was not perturbed. Therefore, the correlation function analysis was applied to the PVDF-rich compositions ($w_{PHB} \leq 0.4$) here.

Fig. 4 shows the one-dimensional correlation functions for the blends crystallized at 70°C. Assuming the corresponding two-phase model, the average crystalline thickness (l_c^{PVDF}), amorphous layer thickness (l_a^{PVDF}), and the most probable value of long period (L^{PVDF}) in the PVDF LS domains can be estimated via simple geometric analysis of $K(z)$, as demonstrated in Fig. 5 [32]. l_c^{PVDF} is given by the intersection between the straight line extended from the self-correlation triangle and the baseline given by $-A$; l_a^{PVDF} is then obtained from $l_a^{PVDF} = L^{PVDF} - l_c^{PVDF}$.

Fig. 6 plots L^{PVDF}, l_c^{PVDF}, and l_a^{PVDF} as a function of blend composition. It can be seen that all three morphological parameters display similar trend, where they increase with PHB composition but level off at $w_{PHB} = 0.2$ for $T_c = 70$ and 125°C or decrease slightly at $w_{PHB} = 0.3$ for $T_c = 146$°C. The crystalline thickness increases slightly (≤3 nm) upon

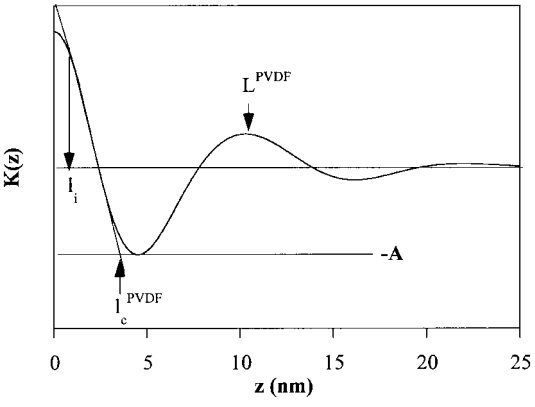

Fig. 5. Determinations of the layer thicknesses in the LSs via the geometric analysis of the Strobl–Schneider's one-dimensional correlation function.

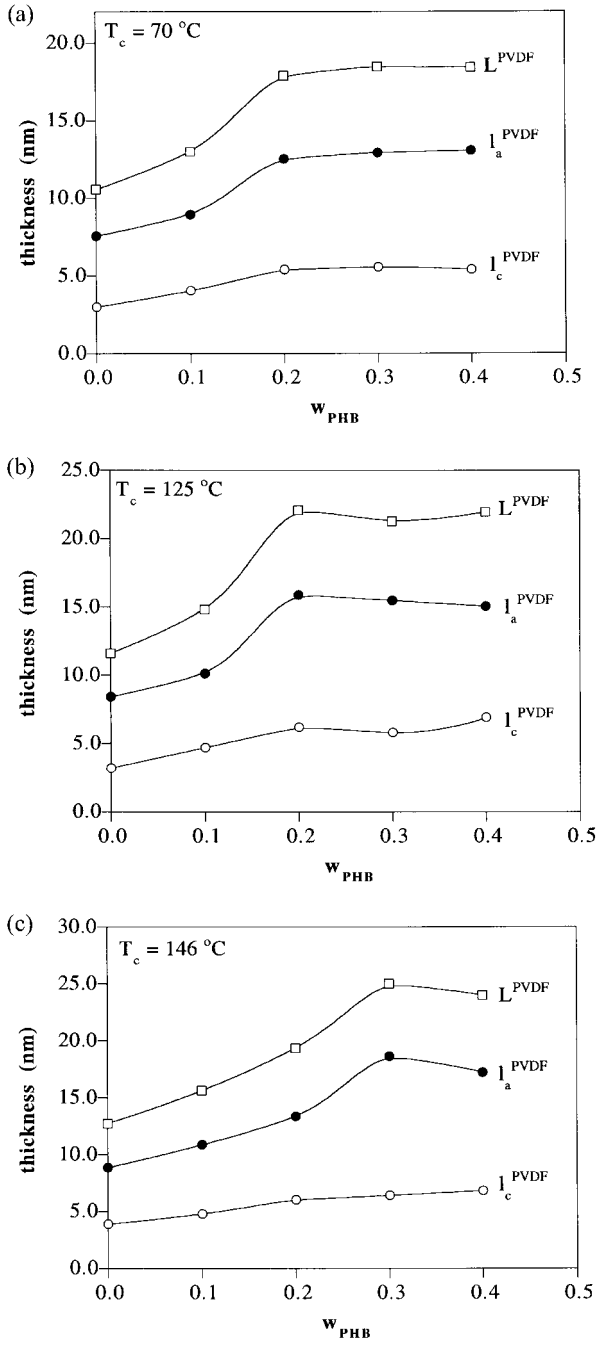

Fig. 6. Composition variations of the crystalline thickness (l_c^{PVDF}), amorphous layer thickness (l_a^{PVDF}), and long period (L^{PVDF}) in the PVDF LS domains of PVDF/PHB crystallized at T_c = (a) 70°C, (b) 125°C, and (c) 146°C.

blending. This can be connected with the assumption of the 'corresponding two-phase model' in deriving l_c^{PVDF} and l_a^{PVDF} from $K(z)$. In this model, the thickness of the crystal/amorphous interphase (l_i) is 'split' into the values of l_c^{PVDF} and l_a^{PVDF}. The interphase thickness can be estimated from the deviation from the self-correlation triangle near $z = 0$ (Fig. 5) [32]. The values of l_i thus obtained are tabulated in Table 1. The interphase thickness appears to

Table 1
Thickness of crystal/amorphous interphase (l_i) estimated from $K(z)$

w_{PHB}	l_i (nm)		
	$T_c = 70°C$	$T_c = 125°C$	$T_c = 146°C$
0.0	0.87	0.83	0.87
0.1	1.05	1.16	1.28
0.2	1.06	1.70	1.76
0.3	1.44	1.46	1.43
0.4	1.58	2.06	2.64

increase with PHB composition, so the inclusion of l_i into l_c^{PVDF} may be responsible for the observed slight increase of crystalline thickness.

l_a^{PVDF} also increases upon blending and the swelling is much larger than the magnitude of l_i; therefore, the swelling of l_a^{PVDF} is attributed to the incorporation of uncrystalline PHB in the IL regions of the PVDF LS domains. This is consistent with the enhancement of scattering intensity observed in Fig. 1. The swelling of l_a^{PVDF} is however not monotonic, as it reaches a saturation at $w_{PHB} = 0.2$ or 0.3. This implies that a portion of PHB was expelled out of the IL regions (i.e. the extralamellar segregation) during the crystallization of PVDF. Based on this observation of extralamellar segregation, the mechanism of dual LS domain formation can be depicted as follows. When the blends were cooled to T_c, crystallization of PVDF occurred prior to that of PHB. There then existed a time period over which PHB was a 'temporary amorphous diluent' with respect to PVDF, and extralamellar segregation of this temporary amorphous diluent was driven by the crystallization of PVDF. The PHB expelled out of the IL regions could accumulate in the regions between the PVDF lamellar bundles (i.e. the interfibrillar regions) or in the interspherulitic regions, and thus created the PHB-rich amorphous domains. The PHB LS domains were formed by the subsequent crystallization of PHB within these amorphous domains.

The absolute invariant (Q) which is related to the degree of phase separation can be obtained from the integrated SAXS intensity

$$Q = \int_0^\infty Iq^2 \, dq. \tag{2}$$

Since the experimentally accessible q range is finite, extrapolation of intensity to both zero and high q is necessary for the integrations. Extrapolation to zero q was accomplished by linear extrapolation and extension to high q was performed using the Porod–Ruland equation [33].

Fig. 7 plots the invariant as a function of composition. It can be seen for the blends that the invariant decreases with increasing T_c. To explain this observation, we approximate the observed invariant to contain three contributions

$$Q = Q_{PVDF} + Q_{PHB} + Q_{PVDF-PHB}, \tag{3}$$

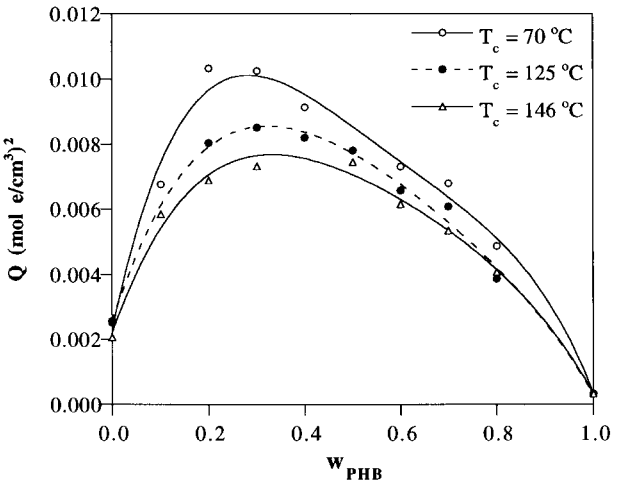

Fig. 7. The SAXS invariants of PVDF/PHB crystallized at $T_c = 70$, 125, and 146°C.

where Q_{PVDF} and Q_{PHB} are the contributions from the individual PVDF and PHB LS domains, respectively, and $Q_{PVDF-PHB}$ is the contribution stemming from the interference between PVDF and PHB LS domains. $Q_{PVDF-PHB}$ should appear at the low-q regions because the size of the LS domains is larger than that of the individual lamellae. The larger the LS domain, the lower the q region where this contribution should appear. In the case, where the LS domains are larger than the length scale corresponding to the minimum accessible q of the typical SAXS instrument (ca. 66 nm for our SAXS system), the contribution of $Q_{PVDF-PHB}$ is undetectable by SAXS. The linear extrapolation to $q = 0$ for the invariant calculation would not accurately describe the scattering profile associated with $Q_{PVDF-PHB}$. The measured Q would then consist of only two contributions, i.e.

$$Q \approx Q_{PVDF} + Q_{PHB}. \tag{4}$$

On the other hand, if the size of the LS domains are in the nanoscopic range, part of $Q_{PVDF-PHB}$ becomes measurable by SAXS. In this case, the measured invariant would contain all three contributions. Based on this model, we can conclude that the LS domain size created at the three T_cs follows the order of T_c (146°C) > T_c (125°C) > T_c (70°C).

The reason why the LS domain size was larger at higher T_c can be rationalized by the disparity in crystallization kinetics between PVDF and PHB. The disparity in crystallization kinetics is the largest at 146°C. At this T_c, PHB was basically an amorphous diluent throughout the crystallization of PVDF. The slow PVDF crystal growth rate and the high PHB chain mobility at this T_c allowed PHB to be expelled by a long distance (e.g. the μm scale) during the crystallization of PVDF. The result was the sequential stacking of PVDF lamellae to extend over a long distance and thus created large PVDF LS domains. At lower T_c such

as 70°C, the disparity in crystallization kinetics diminished. The segregation distance of PHB was limited by its increased crystallization rate, because translational motion was prohibited once the chains crystallize. The restriction in mutual exclusion distance limited the sequential stacking of lamellae to a shorter distance and thus resulted in smaller LS domains. The disparity in crystallization kinetics has also been found to influence the correlation length associated with the LS domains in crystalline/crystalline PEO/PES blends [3].

4. Conclusions

The crystalline/crystalline morphology of PVDF/PHB blends has been investigated by SAXS. For the three T_cs investigated ($T_c = 70$, 125, and 146°C), crystallization of the two components always generated two LS domains with one containing primarily PVDF lamellae and the other consisting of PHB lamellae. Based on the observed T_c dependence of SAXS invariant, it was proposed that larger LS domains could be formed at higher T_c. At high T_c, the disparity in crystallization kinetics between PVDF and PHB was large, so PHB was basically an amorphous diluent throughout the crystallization of PVDF. In this case, PHB could be expelled by a long distance (e.g. the μm scale) during the crystallization of PVDF, so that the sequential stacking of PVDF lamellae could extend over a long distance and thus created large PVDF LS domains.

Acknowledgements

This work is supported by the National Science Council, ROC under grant NSC 89-2216-E-007-014, and also in part by the US Department of Energy under Contract No. DE-AC05-00OR22725 with the Oak Ridge National Laboratory, managed by the UT-Battelle, LLC.

References

[1] Stein RS, Khambatta FB, Warner FP, Russell T, Escala A, Balize E. J Polym Sci Polym Symp 1978;63:313.
[2] Stein RS. Pure Appl Chem 1991;63:941.
[3] Chen HL, Wang SF. Polymer 2000;41:5157.
[4] Cheung YW, Stein RS. Macromolecules 1994;27:2512.
[5] Cheung YW, Stein RS, Lin JS, Wignall GD. Macromolecules 1994;27:2520.
[6] Song HH, Stein RS, Wu D-Q, Ree M, Philips JC, Legrand A, Chu B. Macromolecules 1988;21:1180.
[7] Tashiro K, Stein RS, Hsu SL. Macromolecules 1992;25:1801.
[8] Tashiro K, Izuchi M, Kobayashi M, Stein RS. Macromolecules 1994;27:1221.
[9] Tashiro K, Izuchi M, Kobayashi M, Stein RS. Macromolecules 1994;27:1228.
[10] Tashiro K, Izuchi M, Kobayashi M, Stein RS. Macromolecules 1994;27:1234.
[11] Tashiro K, Izuchi M, Kaneuchi F, Jin C, Kobayashi M, Stein RS. Macromolecules 1994;27:1240.
[12] Wignall GD, Londono JD, Lin JS, Alamo RG, Galante MJ, Mandelkern L. Macromolecules 1995;28:3156.
[13] Tashiro K, Imanishi K, Izumi Y, Kobayashi M, Kobayashi K, Satoh M, Stein RS. Macromolecules 1995;28:8477.
[14] Cheung YW, Stein RS, Wignall GD, Yang HE. Macromolecules 1993;26:5365.
[15] Cheung YW, Stein RS, Chu B, Wu G. Macromolecules 1994;27:3589.
[16] Avramova N. Polymer 1995;36:801.
[17] Penning JP, Manley RStJ. Macromolecules 1996;29:77.
[18] Penning JP, Manley RStJ. Macromolecules 1996;29:84.
[19] Fujita K, Kyu T, Manley RStJ. Macromolecules 1996;29:91.
[20] Liu L-Z, Chu B, Penning JP, Manley RStJ. Macromolecules 1997;30:4398.
[21] Avella M, Martuscelli E. Polymer 1988;29:1731.
[22] Avella M, Martuscelli E, Greco P. Polymer 1991;32:1647.
[23] Avella M, Martuscelli E, Raimo M. Polymer 1993;34:3234.
[24] Liu AS, Liau WB, Chiu WY. Macromolecules 1998;31:6593.
[25] Marand H, Collins M. ACS Polym Prepr 1990;31:552.
[26] Edie SL, Marand H. ACS Polym Prepr 1991;32:329.
[27] Russell TP, Lin JS, Spooner S, Wignall GD. J Appl Crystallogr 1988;21:629.
[28] Barham PJ, Otun EL, Holmes PA. J Mat Sci 1984;19:2781.
[29] Canetti M, Urso M, Sadocco P. Polymer 1999;40:2587.
[30] Lando JB, Olf HG, Peterlin A. J Polym Sci Part A-1 1966;4:941.
[31] Nakagawa K, Ishida Y. J Polym Sci Polym Phys Ed 1973;11:2153.
[32] Strobl GR, Schneider M. J Polym Sci Polym Phys Ed 1980;18:1343.
[33] Ruland WJ. J Appl Crystallogr 1971;4:70.